Nano Energy (▮▮▮▮) ▮, ▮▮▮–▮▮▮

Available online at www.sciencedirect.com

ScienceDirect

journal homepage: www.elsevier.com/locate/nanoenergy

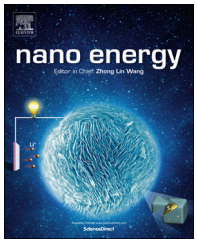

FULL PAPER

Dispersion of carbon nanotubes in aluminum improves radiation resistance

Kang Pyo So[a], Di Chen[b], Akihiro Kushima[a], Mingda Li[a], Sangtae Kim[a], Yang Yang[a], Ziqiang Wang[a], Jong Gil Park[c], Young Hee Lee[c], Rafael I. Gonzalez[d], Miguel Kiwi[d], Eduardo M. Bringa[e], Shao Lin[b,*], Ju Li[a,*]

[a]Department of Nuclear Science and Engineering and Department of Materials Science and Engineering, Massachusetts Institute of Technology, Cambridge, MA 02139, USA
[b]Department of Nuclear Engineering, Texas A&M University, College Station, TX 77845, USA
[c]IBS Center for Integrated Nanostructure Physics, Institute for Basic Science (IBS), Sungkyunkwan University, 440-746, Republic of Korea
[d]Departamento de Fisica, Facultad de Ciencias, Universidad de Chile, Casilla 653, Santiago 7800024, Chile
[e]Facultad de Ciencias Exactas y Naturales, Universidad Nacional de Cuyo, Mendoza 5500, Argentina

Received 6 November 2015; received in revised form 28 December 2015; accepted 21 January 2016

KEYWORDS
Carbon nanotubes;
Irradiation;
Cladding;
Composites;
Aluminum;
Radiation resistance

Abstract

We can mass-produce metal/carbon nanotube (CNT) composites that show improved radiation tolerance. The 0.5 wt% Al+CNT composite showed improved tensile strength without reduction of tensile ductility before radiation, and reduced void/pore generation and radiation embrittlement at high displacements per atom (DPA). Under helium ion irradiation up to 72 DPA, the 1D carbon nanostructures survive, while sp^2 bonded graphene transform to sp^3 tetrahedral amorphous carbon. Self-ion (Al) irradiation converts CNTs to a metastable form of Al_4C_3, but still as slender 1D nanorods with prolific internal interfaces that catalyze recombination of radiation defects, reducing radiation hardening and porosity generation. The 1D fillers may also form percolating paths of "nano-chimneys" that outgas the accumulated helium and other fission gases, and provide an essential solution to the gas accumulation problem.
© 2016 Published by Elsevier Ltd.

Nuclear fission and fusion reactors, nuclear waste containment, nuclear batteries and space explorations demand materials with extraordinary thermomechanical properties and radiation resistance. Radiation can induce severe

*Corresponding authors.
E-mail addresses: lshao@tamu.edu (S. Lin), liju@mit.edu (J. Li).

http://dx.doi.org/10.1016/j.nanoen.2016.01.019
2211-2855/© 2016 Published by Elsevier Ltd.

UNCORRECTED PROOF

damages in materials, including swelling, hardening, creep, embrittlement and irradiation-assisted corrosion [1,2]. The tolerance of radiation damage by structural materials plays a significant role in the safety and economy of nuclear energy [2], as well as the lifetime of nuclear batteries, spaceships and nuclear waste containers, as they are often exposed to long-term radiation [3,4].

Nanostructuring is a key strategy to improve the radiation resistance of materials [5-8]. Carbon nanotubes (CNTs) are well known to be a strong and flexible nanomaterial. If CNTs are uniformly dispersed inside metal as 1D fillers [9-11], its high aspect ratio η (up to 10^8) [12] should create prolific internal interfaces with the metal matrix that may act as venues for the radiation defects to recombine (self-heal). In addition, based on percolation theory and geometrical simulations [13,14], a random 3D network of 1D fillers can form globally percolating transport paths even with diminishing volume fraction $\phi \to 0$, if $\eta \to \infty$. 1D fillers can be efficient for this purpose, considering for example cardiovascular and plant root systems that are 1D transport networks. Helium (alpha particle) accumulation inside materials [15] is a known problem that exacerbates embrittlement and swelling [16]. If the 1D fillers form globally percolating paths of "nano-chimneys" that can outgas the accumulated helium [17] and other fission gases to an external fission-product gettering/trapping system [18], they might provide an essential solution to the problem.

Key questions regarding metal-CNT composite (MCC) in the nuclear environment are:

(1) Does the dispersion of CNTs degrade thermomechanical properties (strength, toughness, thermal conductivity [19], etc.) before irradiation?
(2) Once radiation starts, is radiation embrittlement and swelling reduced (due to self-healing effect of the filler-metal interfaces) in MCC compared to the control metal?
(3) Even if 1D nano-fillers improve (i) and (ii), how stable are these 1D nano-fillers themselves under heavy dose of radiation? Typical radiation exposure to the nuclear fuel cladding material is ~15 DPA (displacements per atom) before they are taken out of the reactor. Core internals in commercial light-water reactors should sustain around 80 DPA after 40 years of plant operations [20], and advanced fast reactors would demand even more.

In this paper we investigate the basic radiation materials science of MCC, in particular Al+CNT composite, using a high-energy ion accelerator to inject He and Al ions which generate atomic displacements in the composite, in lieu of neutrons. We find that in addition to property improvements (i) and (ii), the 1D form factor of nano-fillers does survive up to 72 DPA of He ion irradiation, and also 72 DPA of Al self-ion radiation at room temperature, which is intriguing because every carbon and aluminum atoms are knocked out ~10^2 times, yet the 1D nano-morphologies survive, along with the prolific internal interfaces. The morphological robustness of 1D nano-fillers in non-equilibrium conditions is reminiscent of nanowire growth in chemical vapor deposition that violates equilibrium Wulff construction, and the presence of CNTs in ancient Damascus steel [21] (as the equilibrium phase diagram would indicate that CNTs should be converted to blocky cementite Fe_3C).

We have synthesized Al+CNT composites, as aluminum is cheap and very widely used. Al can be used as the fuel cladding materials in research reactors, as well as containment for nuclear waste, components for robots in radiation environments, etc. It light density may impart significant advantage for space applications. Al has low thermal neutron absorption cross-section of 0.232 barn, above only those of Mg (0.063 barn), Pb (0.171 barn) and Zr (0.184 barn) among structural metals, and high corrosion resistance in water, therefore it is already used widely in low-temperature research reactors [22]. The development of Al+CNT may not only benefit research reactors, but also provide guidance for designing new kinds of cladding materials (e.g., Zr+CNT, Stainless-steel+CNT) that can be used in commercial reactors. Second, Al is used in nuclear battery since it is reflective, and has low production rate of Bremsstrahlung radiation due to low atomic number. Thus it has been recommended for several components in designs of nuclear battery such as shielding, current collector [23] and electrode [24]. Al+CNT will increase the lifetime of nuclear battery because of better radiation resistance. This composite may also alleviate helium accumulation from alpha decay, which is one of the main engineering issues associated with radioisotope thermoelectric generator (RTG) [4].

We have performed accelerator-based ion irradiation tests on Al+CNT (and pure Al control) at room temperature (homologous temperature $T/T_M=0.32$, Al's meting point is $T_M=933.47$ K). At this range, volumetric swelling from void formation becomes prominent when radiation exposure is larger than 10 DPA [2].

Modification of interfaces of 1D nanostructure upon irradiation plays an essential role for MCC properties. Figure 1 provides a schematic illustration of ion beam interaction with CNT. The energies of incoming ions are absorbed and transform CNT structure to rearranged carbon nanostructure, or aluminum carbide nanorods, depending on the ion type and beam energy. The 1D interfaces, if they survive, likely reduce the supersaturation of radiation-generated vacancies, by boosting recombination with self-interstitial atoms (SIA) and interstitial clusters. The light-weight ion irradiation generally generates more "sparse" collision cascades with lower defect density and shorter length compared to heavy ions. Therefore, He ion irradiation causes less Al/C mixing than Al ion irradiation since an interstitial Al atom can quickly find the nearest vacancy of the same chemical species. The CNT undergoes restructuring, making a helical carbon nanostructure, as shown in Figure 1 with a yellow arrow. Irradiation with heavier Al ions, which produce "denser" collision cascades and more Al/C mixing [25], eventually changes the composition of CNT fillers, forming an aluminum carbide phase with 1D nanorod morphology (blue arrow).

For (i), (ii), fabrication of high-quality and low-porosity composite is essential. Achieving uniform CNTs dispersion without inducing degradation to CNTs or Al matrix is the key here. Our specimen preparation consists of three steps (Figure 2A): (step i) declustering of the CNTs on the surface of Al particles, (step ii) encapsulation of the dispersed CNTs and further consolidation into Al particles to form Al-C covalent bonds by spark plasma sintering (SPS), and (step iii) hot extrusion. We used multi-walled carbon nanotubes

UNCORRECTED PROOF

Please cite this article as: K.P. So, et al., Dispersion of carbon nanotubes in aluminum improves radiation resistance, Nano Energy (2016), http://dx.doi.org/10.1016/j.nanoen.2016.01.019

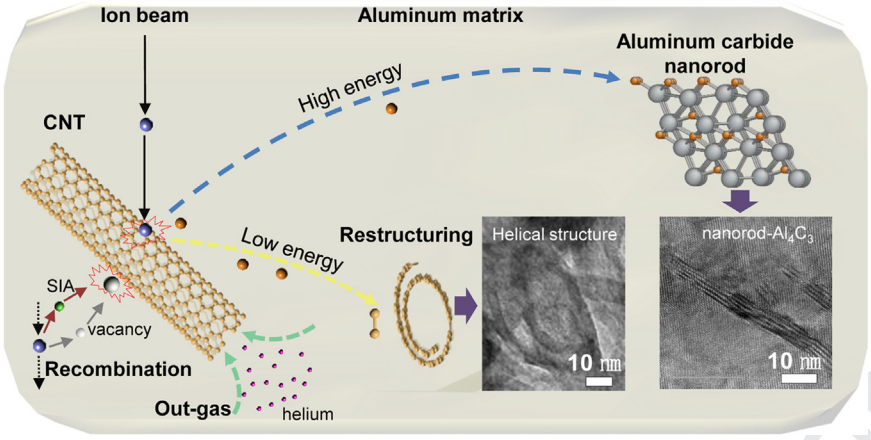

Figure 1 Schematic illustration of shape changes on CNT, recombination, and helium out-gas. Under ion irradiation, the disintegration of CNT and formation of aluminum carbide (blue arrow) from high energy ion and restructuring to helical CNT structure (yellow arrow) from low energy ion are indicated. (For interpretation of the references to color in this figure legend, the reader is referred to the web version of this article.)

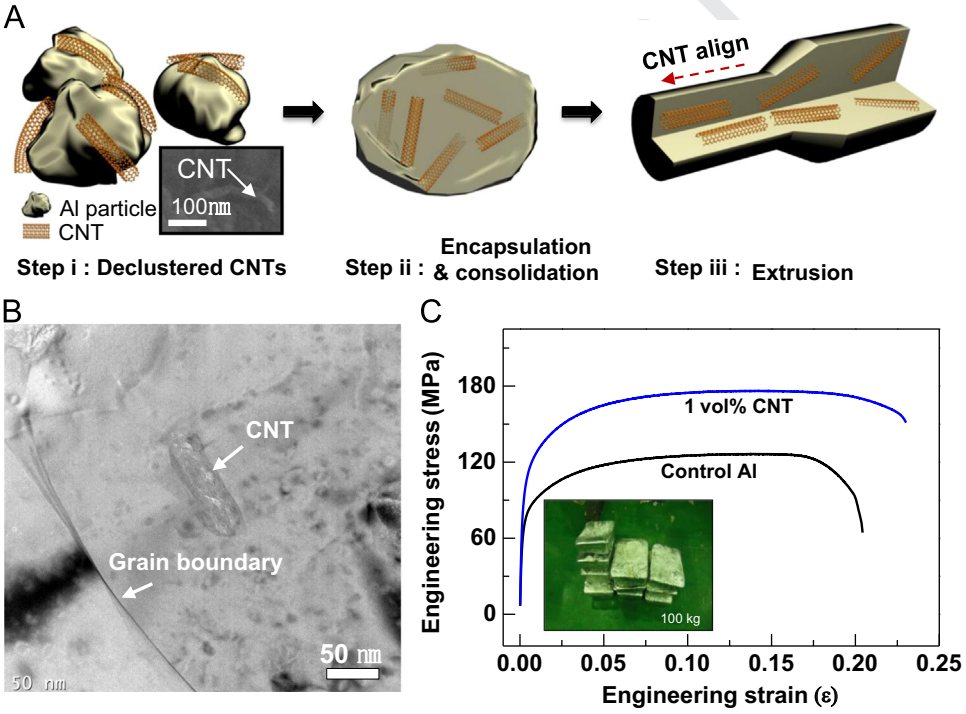

Figure 2 Fabrication process and microstructure/mechanical properties of Al+CNT composites. (A) A schematic representation for the fabrication of Al+CNT composite. (B) Dispersion of CNT inside Al grain in TEM, (C) Stress-strain curve (inset: 100 kg of the Al+CNT composite). Dispersion of CNTs in grain improves the tensile strength without sacrificing ductility.

(MWCNTs) with 10-30 nm in the diameter D and 10 μm in the length L ($\eta \equiv L/D = 300$-1000). The optimized processing conditions are described in detail in Supplementary Online Materials (SOM). This process is industrially scalable, and we have already produced Al+CNT nanocomposite weighing more than 100 kg, as shown in Figure 2C (inset). Cost analysis indicates that its specific weight cost (including raw material cost of MWCNTs and processing costs) should be less than two times the price of bulk-scale Al alloy. The G-mode mapping from confocal Raman indicate the dispersion of CNTs in Figure S1 A and B. Transmission electron microscopy (TEM) observation further verified that CNT embedded inside the Al grain as indicated by the white arrow in Figure 2B. These observations are the evidence that CNTs were highly dispersed after the processing. A bulk specimen for ASTM E8 standard tensile testing, fabricated after hot extrusion, is used for mechanical properties testing. Typical stress-strain curves for the samples with different MWCNTs volume fraction ϕ are shown in Figure 2C. The tensile strength was enhanced by 34% at 1 vol% MWCNTs ($\phi = 0.02$), without sacrificing tensile ductility. As shown in Figure S1C, MWCNTs strands are seen to be protruding out of

Please cite this article as: K.P. So, et al., Dispersion of carbon nanotubes in aluminum improves radiation resistance, Nano Energy (2016), http://dx.doi.org/10.1016/j.nanoen.2016.01.019

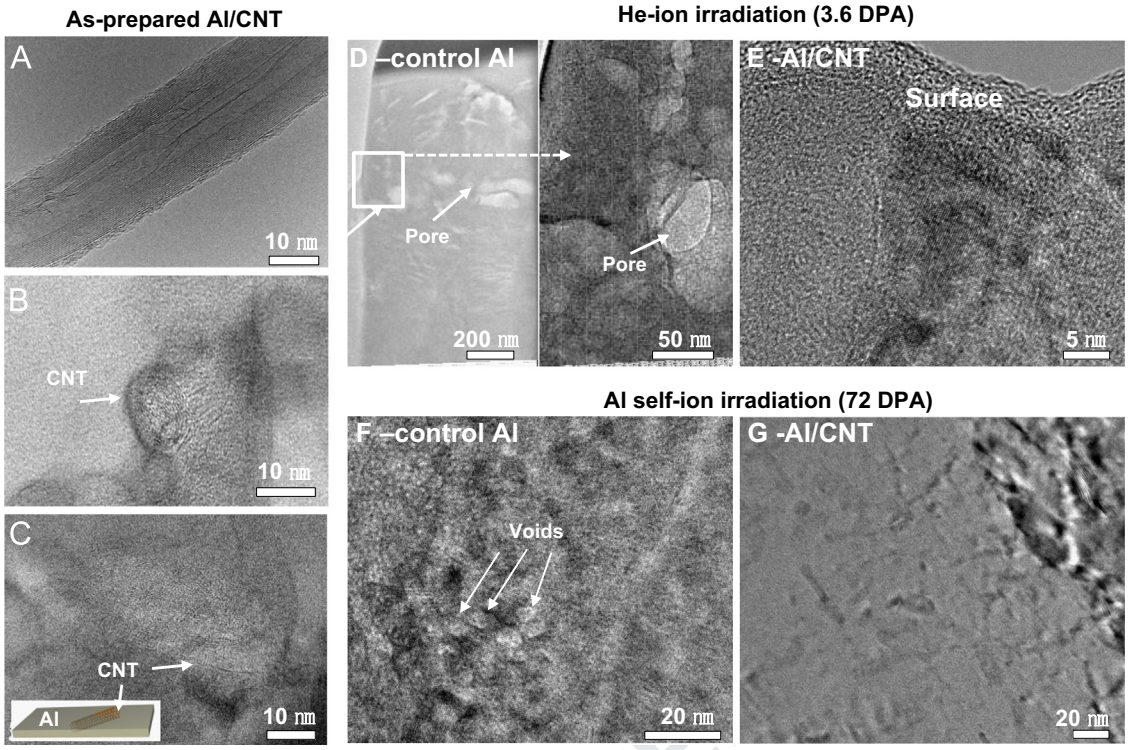

Figure 3 Structural evolution of Al+CNT composite under ion irradiation. TEM image of (A) pristine CNT, (B) and (C) intact wall structure of CNT in Al matrix. Microstructure of (D) control Al and (E) Al+CNT after helium ion irradiation at 3.6 DPA, (F) control Al and (G) Al+CNT after aluminum self-ion irradiation at 72 DPA. Note, no pores were generated by dispersing the 1 vol% of CNT in Al matrix in (E) and (G).

the fractured area, as indicated by the white arrows. This fiber pull-out between CNTs and Al induces load transfer and improves fracture toughness [26].

To test the radiation tolerance of the Al+CNT composite, the sample was irradiated by 100 keV helium ions and 2 MeV aluminum self-ion up to 3.6, 16 and 72 DPA (see SOM), respectively. The results were compared with the pure Al control samples under the same irradiation conditions. The diameter of the inner space and the wall thickness of the MWCNT are 10 nm and 7–10 nm, respectively, as indicated in the TEM image in Figure 3A. The initial geometry does resemble a "nano-chimney". The graphene walls of the CNTs were clearly visible in the TEM images shown in Figure 3B and C, indicating no significant chemical mixing the CNTs. If the MWCNTs are entirely straight and randomly distributed, then analytical modeling and Monte Carlo simulations gives percolation threshold estimate [13,14]:

$$\phi_c \approx \frac{1}{2\frac{L}{D}+3+\pi+\frac{\pi}{2}\frac{D}{L}} \quad (1)$$

which for aspect ratio $\eta \equiv L/D=300$, gives $\phi_c=0.0016$, and for $\eta \equiv L/D=1000$, gives $\phi_c=5\times10^{-4}$. The MWCNT volume fraction we have here is an order of magnitude larger than ϕ_c, therefore the MWCNTs should form a globally percolating network of nano-chimneys. Helium gas is expected to travel facilely in 1D hollow structures like MWCNTs with smooth interior walls.[17]

Figure 3D and E show the control Al samples after 3.6 DPA He-ion irradiation and 72 DPA Al self-ion irradiation, respectively. The irradiation generates nanocavities inside by the aggregation of radiation-induced vacancies, and the positive He gas pressure further stabilizes the bigger cavities compared to Al-ion irradiation. Bubbles appear at just 3.6 DPA in pure Al for He-ion irradiation. The formation of large cavities with diameters ranging 100–200 nm was observed in the control Al (Figure 3D left). The higher magnification indicates that small cavities were also generated (Figure 3D right). In contrast, the Al+CNT 1 vol% sample has no cavity generation at the same DPA (Figure 3E). The higher magnification provides clear evidence of no bubble/void generation at 3.6 DPA He-ion irradiation (Figure 3F) in Al+CNT. Furthermore, no cavity was observed even after 72 DPA Al self-ion irradiation of the Al+CNT (Figure 3G). CNTs dispersed inside Al grain seem to suppress cavity generation completely up to at least 3.6 DPA for He-ion and 72 DPA for Al self-ion radiation, and the answer to (ii) should be positive from the structural point of view.

He-ion radiation to 72 DPA was further carried out to study severe radiation damage condition. Large cavities about 500 nm in diameter were observed in Al without CNTs (Figures 4A and S3A). The surface indicates obvious surface cracking occurred from the volume expansion of the cavities after the irradiation (Figure S2A, bottom). Cavities are also generated in Al+CNT 1 vol% sample at 72 DPA He-ion irradiation, but much smaller than those of control Al (Figures 4B and S3B). The largest cavity is 170 nm in diameter, 20 times smaller in volume than the pore in the control Al. This suggests that the incorporation of MWCNTs in Al suppresses porosity development in severe radiation damage conditions. This obvious reduction of porosity in Al-CNTs composite implies that He gas diffused out of Al matrix

Please cite this article as: K.P. So, et al., Dispersion of carbon nanotubes in aluminum improves radiation resistance, Nano Energy (2016), http://dx.doi.org/10.1016/j.nanoen.2016.01.019

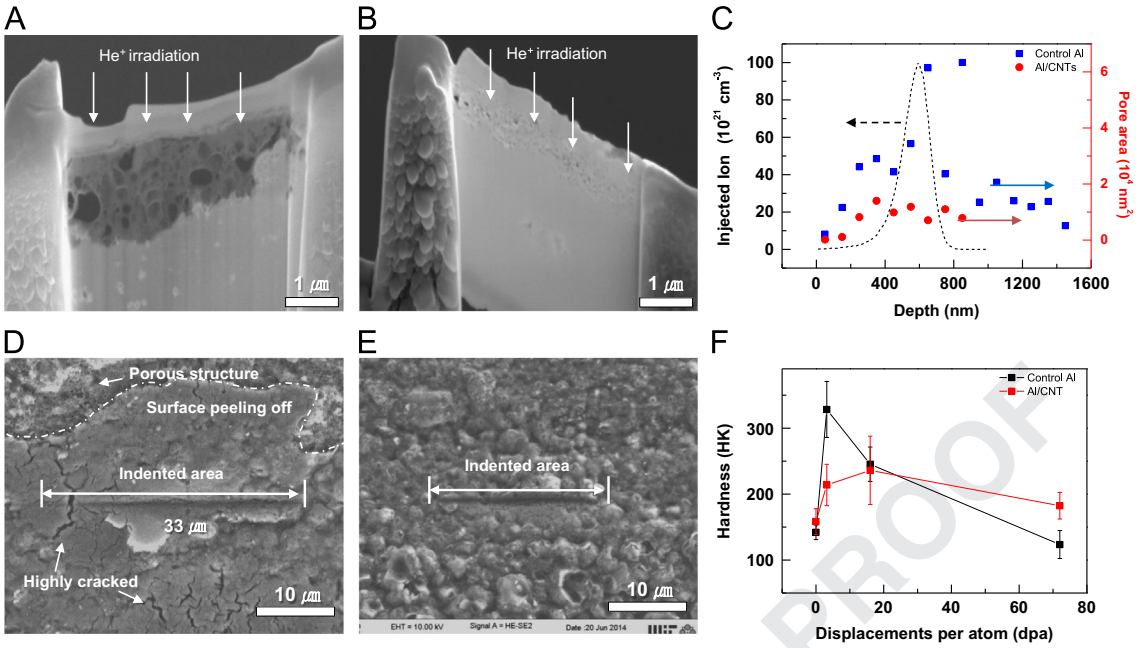

Figure 4 Quantification and mechanical responses of pore generation after 72 DPA helium ion irradiation. SEM image of (A) highly porous control Al and (B) Al+CNT 1 vol%. (C) Injected ion (SRIM) and pore areas versus depth. SRIM is exerted by He ion injection with same experimental parameter. Indented area observation on (D) control Al and (E) Al+CNT composites. Note, highly cracked and porous structure are observed near indented areas in control Al, implying brittle and pore under the surface. (F) Knoop hardness versus DPA.

robustly. Two mechanisms are possible: i) He gas diffused out along the CNT-metal interface, or ii) the interspace and central hollow space inside CNTs acts as 'nano-chimneys' for diffusion of He gas. Since the mechanical strength is enhanced significantly by load transfer associated with strong anchoring of Al onto the CNT surface [9,27], the possibility of the former is small. Therefore, we believe that the globally percolating "nano-chimney" network plays a role for He outgassing.

To quantify the effect of carbon on the radiation damage induced by He ion irradiation in the Al, the stopping and range of ions in matter (SRIM-2013) simulation [srim.org] was performed with/without carbon element in the Al matrix. The carbon content of Al+1 vol% CNT was roughly 0.5 wt%. In the simulation, we uniformly dispersed carbon atoms in the Al matrix to extract the effect of the carbon atoms alone. The maximum DPA is predicted to occur at 534 nm in depth, slightly shallower than the maximum peak (596 nm) of injected He ion. Exactly the same DPA profiles were observed regardless of the presence of carbon, as shown in Figure S4. The 0.5 wt% carbon in Al hence has negligible influence on the helium injection and DPA pro files. Figure 3C shows the relationship between the injected ion/pore generations versus the depth. The simulated damage profiles agree well with the experimentally observed porosity generation profile. However, the absolute cavity area and the size are significantly smaller in the Al +CNT composites than in the control sample. This suggests that the MWCNTs giving high internal interface area is key to the reduced porosity creation. More detailed modeling including the shapes of the MWCNT inclusion and the CNT-Al interactions is necessary to precisely quantify the structural effect, which is beyond the scope of this paper.

If the MWCNTs are randomly dispersed, then the furthest distance between any point of its nearest MWCNTs scales as $L_{\text{furthest}} \propto D\phi^{-1/2}$ (D=diameter). For our 1 vol% MWCNT sample, L_{furthest} should be around 200 nm. This is still an order of magnitude longer than the typical size of a radiation cascade, which is 10-20 nm, therefore the improvement in porosity suggests that porosity development involves length scales quite beyond a single cascade annealing. For comparison, ultra-fine grained austenitic stainless steel with a grain size of 100 nm was recently shown to exhibit 5 times slower void swelling rate up to 80 DPA [7], and L_{furthest} in that case should be around 50 nm if all the grain boundaries (GB) are effective venues for recombination. Compared to that system of "2D nanoengineered" network of GBs [7], our "1D nanoengineered" CNTs/Al has 4 times longer L_{furthest} and 15 times less interfacial area per volume. Yet our system seems to be still similarly effective in cavity suppression.

The above demonstrates aplenty that Al+CNT composite was successful in reducing the structural damage. To show that it leads to property improvement, we conducted micro hardness test to evaluate the change in strength of Al+CNT under radiation exposure. Since the irradiation damage from the ion accelerator was localized beneath the surface within 1 μm depth, we selected the Knoop micro-hardness test to quantify the mechanical behavior in the damaged region. The Knoop micro-hardness test is specially designed for thin film samples. Cracks and porous structure under the surface were observed in the control Al after the Knoop

UNCORRECTED PROOF

Please cite this article as: K.P. So, et al., Dispersion of carbon nanotubes in aluminum improves radiation resistance, Nano Energy (2016), http://dx.doi.org/10.1016/j.nanoen.2016.01.019

indentation, whereas Al+CNT sample showed almost no cracks, as seen in Figure 4D and E, indicating that the Al+CNT sample has less irradiation embrittlement and swelling. The hardness value further verify this observation. The hardness change was measured as a function of DPA as shown in Figure 4F. Note that the hardness increased up to 328 HK at 3.6 DPA in the control Al. In contrast, our Al+CNT nanocomposite, even though it starts out having higher hardness by virtue of higher strength (i), hardens much less compared to control Al (ii). The initial radiation hardening observed in metallic materials results from the obstacles to dislocations, such as point-defect clusters, stacking fault tetrahedra and cavities, generated by radiation. Thus, we again verifies that our "1D nanoengineered" Al+CNT has better radiation tolerance (specifically radiation hardening and embrittlement) compared to the reference control Al.

However, once above 3.6 DPA, the Knoop hardness of control Al decreased with increasing helium ion irradiation dose. This phenomenon could be explained by the severe porosity development which reduced the apparent density of materials. The cavity volume fraction in control Al reached 25% at 72 DPA (Figure 4A). The increasing volume of pores cause the transition from hardening to softening [28], and will result in exceptionally poor toughness as tensile fracture is very sensitive to the size of the largest flaw. In contrast, the cavity volume fraction reached only 4.7% for Al+CNT at 72 DPA, with the largest pore 20 times smaller in volume (Figure S3A and B). Also, the maximum value of the hardness in Al+CNT was reached at 16 DPA (5 times larger dose than control Al), and the 240 HK peak hardening value was much lower than that of the control Al. We are thus confident that the mechanical properties of Al+CNT is more tolerant of both low and high doses of radiation.

High-resolution TEM (HRTEM) was performed on the post-irradiated Al+CNT, as shown in Figure 5A and B. Several tubular cross-sectional structures near each pore were observed (Figure 5A). The tubular structure is still retained after 72 DPA He-ion radiation. Some of the tubular walls merged with each other and the helical shapes were also found, as shown in Figure 1 [29]. Thus, the 1D nano-fillers maintain its general tubular morphology under the He ion irradiation (which generates sparser cascades). Raman spectroscopy indicates quite drastic changes in atomic bonding inside the tubules at higher DPA He-ion irradiation, as confirmed from Raman spectra of D and G bands in Figure 5C. The strong signal near 1440 cm^{-1} corresponds to tetrahedral amorphous carbon (ta-C) with highest sp^3 content (80-90%) [30]. Electron energy loss spectroscopy (EELS) mapping in TEM shows the region with a high carbon concentration (20 nm in width) corresponding to the original diameter of the CNT (Figures 3A and S6B). The sp^3/sp^2 mapping results (Figure S6C and D) indicate strong sp^3 signal at the region of high carbon concentration (see SOM for detail). The observations suggest that the carbon tubular nanostructures observed in TEM are composed of

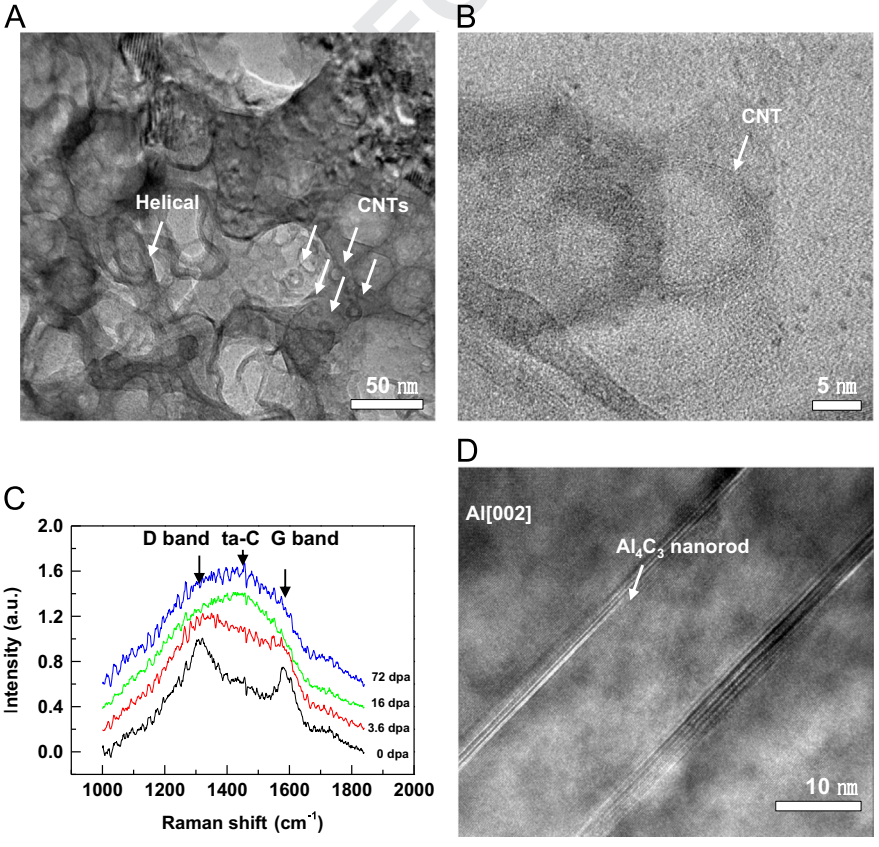

Figure 5 Structure of CNT after 72 DPA irradiation. (A) Traces and (B) wall structure of CNTs after helium ion irradiation, and (C) Raman spectrum at different DPA. (D) Al_4C_3 nanocarbide under 72 DPA Al self-ion irradiation. *Note:* the structure of Al_4C_3 nanocarbide is described in supplementary (Figure S8).

Please cite this article as: K.P. So, et al., Dispersion of carbon nanotubes in aluminum improves radiation resistance, Nano Energy (2016), http://dx.doi.org/10.1016/j.nanoen.2016.01.019

diamond-like carbon with tetrahedral amorphous sp^3 bonding, instead of aluminum carbide (Al_4C_3) which should form according to the equilibrium phase diagram below 2160 °C [31].

In reference to pure Al and graphite, the Gibbs free energy of formation for the stable phase of Al_4C_3 (rhombohedral) is −194.4 kJ/mol at room temperature [31] or −2.01 eV per Al_4C_3 formula unit. On a per carbon basis, it is not as high as ZrC (−2.14 eV per ZrC [32]), but is comparable to SiC (−0.76 eV per SiC) and much higher than cementite (−0.18 eV per Fe_3C). So the fact that much of the carbon nanostructures survive without forming the carbide after 72 DPA He-ion irradiation is somewhat surprising. On the other hand, the conversion of sp^2 bonding of carbon in CNTs to sp^3 of ta-C agrees with the previous understanding of radiation damage of carbon [33].

Aluminum self-ion irradiation with higher energy of 2 MeV (20 × that of helium ion) which create denser cascades [25] eventually disintegrates the pure carbon nanostructure, and generates slender Al_4C_3 nanocarbides, as shown in Figures 5D and S8, and illustrated in Figure 1. The denser cascade provides higher probability to mix carbon with the matrix aluminum atoms. The 1D nature of Al_4C_3 nanocarbides was confirmed in a series of tilting images inside the TEM. The electron diffraction along Al [001] zone axis on the nanocarbide shows that the new structure embedded in the matrix is not the rhombohedral phase of Al_4C_3 (ICSD number 14397), but a metastable triclinic phase (materialsproject.org mp632442). Density functional theory calculations reveal that, intriguingly, this metastable Al_4C_3 nanocarbide has higher formation energy of about 2.8 eV per unit formula above the rhombohedral phase ground state. This energetic metastability is about 1.877 MJ/kg, almost half of the detonation energy density of TNT. We have also determined that many distinct lattice orientation relationships are present between the newly formed Al_4C_3 and Al matrix, with semicoherent and incoherent interfaces based on high-resolution TEM observations. The 1D nanocarbides likely benefit energetically from the interfacial energy considerations with the matrix, which otherwise would be considered high energy in bulk form. Figure 5D is quite remarkable in that it shows two Al_4C_3 nanocarbides running parallel to each other, separated by ~20 nm, on the order of *D* of the original MWCNTs. We surmise these two nanocarbides are decomposition products from the same MWCNT, that originally ran in the same direction, like "fly in amber". The high-energy self-ion radiation destroyed the hollowness of the MWCNT and backfilled it with Al, but vestiges of the original 1D nanostructures remain like fossil record. The nanocarbides are thus templated by the original carbon nanostructures, and this *in situ* formation could be a new paradigm for creating radiation-tolerant nanodispersion-strengthened metals.

In summary, we can mass-produce Al-CNT nanocomposite cheaply, at 100 kg scale and at no more than 2 × the cost. With regard to question (i), CNTs improve strength while maintaining tensile ductility. Our helium and aluminum ion irradiation experiments demonstrate that uniform dispersion of CNT reduces radiation hardening and embrittlement. These evidences indicate that the answer to (ii) is affirmative, due to efficient defect recombination at the incoherent CNT-metal interfaces. Detailed microstructural characterizations further demonstrate that the prolific 1D slender form factors are surprisingly robust under radiation, and survive up to 72 DPA of He-ion and Al-ion irradiations, answering question (iii). Therefore, Al-CNT nanocomposite satisfies all three main concerns (i), (ii) and (iii), providing a paradigm to improve components in nuclear fission and fusion reactors, nuclear waste containment, nuclear batteries and space explorations that demand materials with extraordinary thermomechanical properties and radiation resistance.

Acknowledgment

We acknowledge support by NSF DMR-1410636 and DMR-1120901, and U.S. Department of Energy, Office of Basic Energy Sciences, under Grant no. DE-SC0006725. This research was also supported by Institute for Basic Science (IBS-R011-D1) and Basic Science Research Program through the National Research Foundation of Korea (NRF) funded by the Ministry of Education, Science and Technology (NRF-2013R1A6A3A03064138). EMB thanks support from PICT0092 and a SeCTyP-UNCuyo Grant. RG and MK thanks the support from Fondo Nacional de Investigaciones Cientificas y Tecnologicas (FONDECYT, Chile) under Grants #3140526 (RG), #1120399 and 1130272 (MK), and Center for the Development of Nanoscience and Nanotechnology CEDENNA FB0807 (RG and MK)

Appendix A. Supplementary material

Supplementary data associated with this article can be found in the online version at http://dx.doi.org/10.1016/j.nanoen.2016.01.019.

References[1]

[1] E.M. Bringa, et al., Nano Lett. 12 (2012) 3351–3355. http://dx.doi.org/10.1021/nl201383u.
[2] S.J. Zinkle, J.T. Busby, Mater. Today 12 (2009) 12–19.
[3] L.S. Novikov, et al., J. Surf. Investig. - X-Ray 3 (2009) 199–214. http://dx.doi.org/10.1134/S1027451009020062.
[4] T. Wacharasindhu, J.W. Kwon, D.E. Meier, J.D. Robertson, Appl. Phys. Lett. 95 (2009) 014103. http://dx.doi.org/10.1063/1.3160542.
[5] I.J. Beyerlein, et al., Mater. Today 16 (2013) 443–449. http://dx.doi.org/10.1016/j.mattod.2013.10.019.
[6] S. Wurster, R. Pippan, Scr. Mater. 60 (2009) 1083–1087. http://dx.doi.org/10.1016/j.scriptamat.2009.01.011.
[7] C. Sun, et al., Sci. Rep. 5 (2015) 7801. http://dx.doi.org/10.1038/srep07801 http://www.nature.com/srep/2015/150115/srep07801/abs/srep07801.html#supplementary-information.
[8] G.R. Odette, JOM 66 (2014) 2427–2441. http://dx.doi.org/10.1007/s11837-014-1207-5.
[9] K.P. So, et al., Acta Mater. 59 (2011) 3313–3320. http://dx.doi.org/10.1016/j.actamat.2011.01.061.
[10] K.P. So, et al., Compos. Sci. Technol. 74 (2013) 6–13. http://dx.doi.org/10.1016/j.compscitech.2012.09.014.
[11] S.R. Bakshi, D. Lahiri, A. Agarwal, Int. Mater. Rev. 55 (2010) 41–64. http://dx.doi.org/10.1179/095066009X12572530170543.
[12] X. Wang, et al., Nano Lett. 9 (2009) 3137–3141. http://dx.doi.org/10.1021/nl901260b.

[1] ⟨http://li.mit.edu/S/dc/Paper/⟩.

ARTICLE IN PRESS

[13] S.I. White, et al., Adv. Funct. Mater. 20 (2010) 2709–2716. http://dx.doi.org/10.1002/adfm.201000451.
[14] R.M. Mutiso, M.C. Sherrott, J. Li, K.I. Winey, Phys. Rev. B 86 (2012) 214306 87, doi:Artn 019902 1103/Physrevb.87.019902 (2013).
[15] A. Kashinath, A. Misra, M.J. Demkowicz, Phys. Rev. Lett. 110 (2013) 086101.
[16] G.R. Odette, M.J. Alinger, B.D. Wirth, Annu. Rev. Mater. Res. 38 (2008) 471–503. http://dx.doi.org/10.1146/annurev.matsci.38.060407.130315.
[17] H. Verweij, M.C. Schillo, J. Li, Small 3 (2007) 1996–2004. http://dx.doi.org/10.1002/smll.200700368.
[18] A. Schwartz, et al., Postirradiation Examination of Peach Bottom Fuel Elements E05-05 and C05-05 and Related Analyses, Gulf General Atomic, U. S. Atomic Energy Commission, 1969.
[19] J. Li, L. Porter, S. Yip, J. Nucl. Mater. 255 (1998) 139–152. http://dx.doi.org/10.1016/s0022-3115(98)00034-8.
[20] S.J. Zinkle, G.S. Was, Acta Mater. 61 (2013) 735–758. http://dx.doi.org/10.1016/j.actamat.2012.11.004.
[21] M. Reibold, et al., Nature (2006)286 ⟨http://www.nature.com/nature/journal/v444/n7117/suppinfo/444286a_S1.html⟩.
[22] K. Farrell, Mater. Perform. Corros./Waste Mater. 5 (2012) 143–175.
[23] Google Patents, 1958.
[24 H.R. Shanks, Google Patents, 1998.
[25] Rafael I. Gonzalez, et al., Metal-Nanotube Composites as Radiation Resistant Materials, (to be submitted)(2015).
[26] B. Boesl, D. Lahiri, S. Behdad, A. Agarwal, Carbon 69 (2014) 79–85. http://dx.doi.org/10.1016/j.carbon.2013.11.061.
[27] K.P. So, et al., Prevention of Ductility Reduction in CNT-Reinforced Aluminum via Multi-Step Rupturing Process, 2016.
[28] M.F. Ashby, R.F.M. Medalist, MTA 14 (1983) 1755–1769. http://dx.doi.org/10.1007/bf02645546.
[29] M. Terrones, et al., Phys. Rev. Lett. 89 (2002) 075505.
[30] A.C. Ferrari, J. Robertson, Phil. Trans. R. Soc. Lond. A 362 (2004) 2477–2512. http://dx.doi.org/10.1098/rsta.2004.1452.
[31] C. Qiu, R. Metselaar, J. Alloy. Compd. 216 (1994) 55–60. http://dx.doi.org/10.1016/0925-8388(94)91042-1.
[32] J. Li, D. Liao, S. Yip, R. Najafabadi, L. Ecker, J. Appl. Phys. 93 (2003) 9072–9085. http://dx.doi.org/10.1063/1.1567819.
[33] F. Banhart, Rep. Prog. Phys. 62 (1999) 1181–1221, http://dx.doi.org/10.1088/0034-4885/62/8/201.

UNCORRECTED PROOF

Please cite this article as: K.P. So, et al., Dispersion of carbon nanotubes in aluminum improves radiation resistance, Nano Energy (2016), http://dx.doi.org/10.1016/j.nanoen.2016.01.019